# Modelling of nonlinear light up-conversion from intense femtosecond laser pulses

**David Amorim (University of Glasgow)**

DESY Summer Student Programme 2023
Group: Attosecond Science (CFEL-ATTO)
Institute: Centre for Free-Electron Laser Science (CFEL)
Supervisor: Josina Hahne

**Abstract.** Ultrashort ultraviolet (UV) laser pulses can be produced via nonlinear optical processes in noble gasses based on few-femtosecond near-infrared (NIR) input pulses. Numerical simulations of these effects were implemented using the propagation solver *Luna.jl*. The simulated UV spectra for Argon and Neon agree qualitativelyl with measured data across different pressures and beam powers. The simulations could be used to show that ionisation-induced self-steepening contributes to spectral broadening and pulse compression, in agreement with similar studies in the literature. It was further demonstrated that using chirped NIR input pulses can increase the spectral bandwidth. The simulations also supported experimental data on the improved performance of a new gas chip design.

With further modifications and extensions, the simulations presented here could form the basis of a robust framework to complement experimental results and aid experimental design by exploring the effects of changing various experimental parameters.

## 1. Introduction

The electronic motion associated with chemical reactions and atomic energy transitions takes place on femotsecond ($1\text{fs} = 10^{-15}$s) to attosecond ($1\text{as} = 10^{-18}$s) time scales. Time-resolved imaging of molecular dynamics therefore requires ultrashort laser pulses in the few-femtosecond regime. An important type of electronic motion is that excited by the absorption of ultraviolet (UV) radiation: a variety of biochemical processes, such as DNA damage, are known to be caused by UV excitation. Generating few-femtosecond UV pulses for time-resolved measurements of UV-excited molecules plays a crucial part in further understanding and eventually controlling these effects.

The CFEL-ATTO group at DESY produces ultrashort UV pulses in the femtosecond regime via third-harmonic generation (THG) in a gas cell [1]. This process is sensitive to a large range of parameters which affect the duration and energy of the generated UV pulse. Numerical simulations of the interactions between the laser pulse and the gas can therefore be advantageous to better understand how THG takes place and how it is affected by the experimental conditions.

This report summarises the work carried out as part of a DESY Summer Student project focussed on producing simulations of the THG process. The simulations were mainly carried out using the propagation solver *Luna.jl* ([2]) while the *COMSOL Multiphysics* software was used to model the gas density distribution. The aim of the simulations was to reproduce the experimental conditions in the gas, in order to study which effects dominate the THG process and the shaping of the UV pulse. Further, parameter scans were simulated to investigate how changes to different variables in the experimental set-up affect the output pulse. This included comparing the performance of a new fused silica chip used to confine the gas to a previous design.

## 2. Background

This section gives a brief overview of key properties of ultrashort (femtosecond) laser pulses, THG and other relevant nonlinear optical effects, as well as the differential equation describing the propagation of ultrafast laser pulses. An in-depth treatment of these topics can be found in textbooks like [3, 4].

The final subsection then presents the experimental conditions of UV generation, which the simulations aim to replicate.

### 2.1. Ultrashort Laser Pulses

An ultrashort laser pulse can be described as a carrier wave at carrier frequency $\omega_0$ with an amplitude modulated by an envelope function. In the femtosecond domain the envelope may only contain a few cycles of the carrier wave. Using the analytic representation of the electric field vector the time-domain representation of an ultrashort laser pulse can be written as

$$\mathbf{E}(t,\mathbf{r}) = \mathbf{A}(t,\mathbf{r})e^{i[\omega_o t+\phi(t)]}, \tag{1}$$

where $\mathbf{A}(t, \mathbf{r})$ represents the envelope function and $\phi(t)$ is the temporal phase. The vectorial nature of the envelope takes into account the polarisation of the pulse. Similarly, the frequency-domain representation is

$$\mathbf{E}(\omega, \mathbf{r}) = \mathbf{A}'(\omega, \mathbf{r})e^{i\varphi(\omega)}, \qquad (2)$$

where $\varphi(\omega)$ is the spectral phase. Note that the effect of the carrier term in the frequency domain is merely a shift along the frequency axis and can be thus be absorbed in the definition of $\omega$.

The spectral and temporal phase are commonly expanded as Taylor-series, with the notation $\phi_n \equiv \frac{\partial^n \phi}{\partial t^n}$ and $\varphi_n \equiv \frac{\partial^n \varphi}{\partial \omega^n}$ used to denote the series coefficients. The zeroth-order terms of both expansions are the same, $\phi_0 = \varphi_0$, and correspond to the carrier-envelope phase (CEP), also known as the absolute phase. The CEP desribes the phase difference between the carrier and the envelope and is particularly relevant for few-cycle pulses. A laser pulse with no terms in $\varphi(\omega)$ higher than $\varphi_0$ is said to be transform-limited. A pulse is said to be chirped if there are nonlinear terms in $\phi(t)$ or $\varphi(\omega)$.

The presence of chirp can result in both spectral and temporal broadening of the pulse envelope. A convenient measure of chirp is therefore the so-called time-bandwidth product $\Delta\omega\Delta t$, where $\Delta\omega$ is the full-width half-maximum (FWHM) of $\mathbf{A}'(\omega, \mathbf{r})$ and $\Delta t$ the FWHM of $\mathbf{A}(t, \mathbf{r})$. It can be shown that the time-bandwidth product is minimised for transform-limited, i.e. unchirped, pulses.

The effects on a laser pulse when travelling through a medium can be described via additional terms in the spectral phase: $\varphi(\omega) \to \varphi(\omega) + [\beta(\omega) + i\alpha(\omega)]L$, where $L$ corresponds to the distance travelled in a medium, $\beta(\omega)$ is the propagation coefficient, and $\alpha(\omega)$ the absorption coefficient. The latter term represents an attenuation of the pulse while the former has the effect of introducing chirp (provided the Taylor-expansion of $\beta(\omega)$ has non-zero terms higher than $\beta_1$). Note that depending on the signs of the quantities involved, the chirp due to $\beta(\omega)$ will either increase or compensate the existing chirp on the pulse. Thus, an initially positively chirped pulse will further broaden upon propagation through a normally dispersive medium while a negatively chirped pulse will be compressed. The opposite effect is observed in anomalously dispersive media.

### 2.2. Nonlinear Optics and THG
For most materials, the polarisation response to an electric field of moderate intensity is linear. The peak intensities reached in ultrashort laser pulses are large enough, however, for this approximation

to become invalid and nonlinear polarisation components to appear. The resulting polarisation can then be represented as a combination of a linear and a nonlinear term: $\mathbf{P}(t, \mathbf{r}) = \mathbf{P}^{\mathrm{L}}(t, \mathbf{r}) + \mathbf{P}^{\mathrm{NL}}(t, \mathbf{r})$, where spatial dependencies have been left implicit.

The linear polarisation is given by the familiar expression $\mathbf{P}^{\mathrm{L}}(t, \mathbf{r}) = \epsilon_0 \chi_e \mathbf{E}(t, \mathbf{r})$, where $\chi_e$ is the (linear) electric susceptibility. The nonlinear term, $\mathbf{P}^{\mathrm{NL}}(t, \mathbf{r})$, on the other hand, is less trivial. It can be approximated using a perturbative approach in combination with a term that takes into account the effects of photoionisation, which is non-perturbative:

$$\mathbf{P}^{\mathrm{NL}}(t, \mathbf{r}) = \epsilon_0 \sum_{n=2} \chi^{(n)}[\mathbf{E}(t, \mathbf{r})]^n + \mathbf{P}^{\mathrm{ion}}(t, \mathbf{r}), \quad (3)$$

where $\chi^{(n)}$ is the $n$-th order electric susceptibility. Note that for gases the assumption that the higher-order susceptibilities are frequency-independent scalars is a good approximation. Further note that the series expansion starts at the quadratic term as the linear term is contained in $\mathbf{P}^{\mathrm{L}}(t, \mathbf{r})$.

In centrosymmetric media such as gases all even-order susceptibilities necessarily vanish, so that the dominant term in the expansion is the third-order term. Higher-order contributions can be neglected to a good approximation, so that (3) becomes

$$\mathbf{P}^{\mathrm{NL}}(t, \mathbf{r}) = \epsilon_0 \chi^{(3)}[\mathbf{E}(t, \mathbf{r})]^3 + \mathbf{P}^{\mathrm{ion}}(t, \mathbf{r}), \quad (4)$$

where $[\mathbf{E}(t, \mathbf{r})]^3 \equiv \mathbf{E}(t, \mathbf{r})|\mathbf{E}(t, \mathbf{r})|^2$. The first term in (4) is known as the Kerr term and its presence leads directly to THG. This can be seen when considering an oscillating electric field $\mathbf{E}(t, \mathbf{r}) = \hat{\mathbf{E}}(t, \mathbf{r})\cos(\omega t)$. The resulting Kerr response then is

$$\begin{aligned}\mathbf{P}^{\mathrm{Kerr}}(t, \mathbf{r}) &= \epsilon_0 \chi^{(3)}[\hat{\mathbf{E}}(t, \mathbf{r})]^3 \cos^3(\omega t) \\ &= \frac{\epsilon_0}{4}\chi^{(3)}[\hat{\mathbf{E}}(t, \mathbf{r})]^3 \left\{\cos(3\omega t) + 3\cos(\omega t)\right\}.\end{aligned}$$
$$(5)$$

The first summand in (5) corresponds to a field contribution oscillating at the frequency $3\omega$. Thus, a pump wave at the fundamental frequency $\omega$ will generate a co-propagating frequency-tripled field. This process can be identified as THG. Note that THG is just once instance of a range of nonlinear optical effects which result in the generation of higher-frequency waves from a driving field, generally known as frequency up-conversion.

The intensity of the third harmonic is determined by the value of $\chi^{(3)}$ in a given medium as well as by the intensity of the driving field. This also implies that, since the intensity of the fundamental pulse is highest at the peak of the envelope, THG conversion is more efficient there so that the third

harmonic pulse is narrower in time than the input pulse by a factor of $\sim \sqrt{3}$.

A further factor to consider is that the third harmonic is generated in-phase with the driving wave at each point in the nonlinear medium. Thus, in dispersive media there will be phase differences between third harmonic contributions generated at different points along the crystal. This can result in destructive interference and thus lower the THG conversion efficiency.

The second summand in (5), corresponding to polarisation response at the fundamental frequency, is also significant: its effect is a correction term in the refractive index that is proportional to the intensity of the driving field. This intensity-dependent refractive index (IDRI) produced by the Kerr term has important implications for the propagation of laser pulses in nonlinear media. These self-steepening: self-steepening describes the effect of the peak of the pulse experiencing, due to the IDRI, a different group velocity in a dispersive medium than the wings. This results in the leading edge of the pulse or, in the case of anomalous dispersion, the trailing edge, to get steeper on propagation, corresponding to temporal compression and spectral broadening.

After having considered the effects of the Kerr term in the previous paragraphs, we now turn to the second term in (3): the nonlinear polarisation due to photoionisation. The highly energetic driving pulse can ionise the atoms or molecules in the nonlinear medium, resulting in the presence of free electrons. This has a two-fold effect on pulse propagation and THG. On the one hand, the pump field is depleted since it must overcome the atomic ionisation potential, so that less energy is available to drive THG. On the other hand, the freed electrons also interact electromagnetically with the fundamental and third harmonic fields, which results in spatio-temporal reshaping of the pulses. Thus, despite ionisation limiting the achievable third harmonic pulse energy, it can aid in further shortening the generated pulses.

The theoretical treatment of $\mathbf{P}^{\text{ion}}(t, \mathbf{r})$ is significantly more sophisticated than that of the Kerr term. As is derived in [5]:

$$\frac{\partial}{\partial t}\mathbf{P}^{\text{ion}}(t, \mathbf{r}) = \frac{I_p}{\mathbf{E}(t)}\frac{\partial n_e}{\partial t} + \frac{e^2}{m_e^2}\int_{-\infty}^{t} n_e(t')\mathbf{E}(t')dt',$$
(6)

where $n_e(t)$ is the number of free electrons at any point in time, $I_p$ is the ionisation potential, and $e$, $m_e$ represent the electron charge and mass, respectively. The value of $n_e(t)$ can be found from

$$\frac{\partial n_e}{\partial t} = (n_e - n_0)W(\mathbf{E}),$$
(7)

where $n_0$ is the initial number of neutral atoms and $W(\mathbf{E})$ is the ionisation rate, which can be calculated from the so-called ADK model of tunnel ionisation or the PPT model, which is more sophisticated but also more computationally expensive.

### 2.3. The Unidirectional Pulse Propagation Equation

A variety of different differential equations can be used to describe the propagation of laser pulses. Many of them are derived under the slowly-varying- envelope assumption (SVEA), which approximates the carrier wave to change significantly more quickly in space and time than the pulse envelope. The SVEA does not hold for ultrashort pulses, however, and hence many commonly used pulse propagation equations are not suitable for the study of few-femtosecond pulses. The unidirectional pulse propagation equation (UPPE) is derived directly from Maxwell's equations without additional approximations, see [6], and therefore can be applied to ultrashort pulses. It is the differential equation used by *Luna.jl* to simulate laser pulse propagation. This section gives a brief overview of the UPPE and how it is solved in *Luna.jl*. For more details on numerical solutions of the UPPE see the *Luna.jl* documentation, [2], as well as [7].

The general form of the UPPE for a laser pulse of frequency $\omega$ travelling in the $z$-direction is

$$\frac{\partial}{\partial z}\mathbf{E}(\omega, \mathbf{k}_\perp, z) = \mathcal{L}(\omega, z)\mathbf{E}(\omega, \mathbf{k}_\perp, z)$$
$$+ \frac{i\omega}{N}\mathbf{P}^{\text{NL}}(\omega, \mathbf{k}_\perp, z),$$
(8)

where $\mathbf{E}(\omega, \mathbf{k}_\perp, z)$ is the reciprocal-space electric field amplitude in the frequency domain, $\mathbf{k}_\perp$ is the transverse spatial frequency vector, $\mathcal{L}(\omega, z)$ is a linear operator describing dispersion and absorption, $\mathbf{P}^{\text{NL}}(\omega, \mathbf{k}_\perp, z)$ is the frequency-domain nonlinear polarisation in reciprocal space and $N$ is a normalisation factor.

For a laser pulse propagating in a gas, not confined by a fibre or waveguide, the linear operator $\mathcal{L}(\omega, z)$ is given by

$$\mathcal{L}(\omega, z) = i\left(\beta(\omega, z) - \frac{\omega}{v}\right) - \frac{1}{2}\alpha(\omega, z),$$
(9)

where $\beta(\omega, z)$ is the propagation coefficient of the gas, $v$ is a reference frame velocity (chosen to be the group velocity at the central wavelength $\lambda_0$), and $\alpha(\omega, z)$ is the absorption coefficient of the gas.

As is seen in (4) and (6), the nonlinear polarisation is naturally calculated from the electric field in real space and the time domain. Thus,

3

numerically solving the UPPE, which lives in reciprocal space and the frequency domain, requires a cycle of temporal Fourier transforms into and out of the frequency domain as well as transverse spatial transforms into and out reciprocal space at each step. The choice of transverse spatial transform is determined by the geometry of the system.

Since the beam and the gas channel it propagates through for UV generation are approximately radially symmetric, a zeroth-order Hankel transform is chosen as the transverse spatial transform. This is mathematically equivalent to a transverse spatial Fourier transform in Cartesian coordinates but is computationally more efficient, as the Hankel transform exploits the symmetry and only involves integration in the radial direction, whereas the transverse spatial Fourier transform is two-dimensional.

## 2.4. Experimental Conditions

The CFEL-ATTO group generates few-femtosecond UV laser pulses via THG in a gas cell. This is driven by a pulsed near-infrared (NIR) Ti:sapphire laser with a central wavelength of 800nm and a repetition rate of 1kHz. Various fibre-based pulse-shaping and compression techniques are used to produce NIR pulses with a duration of around 5fs and a pulse energy of up to 3mJ. A fraction of the NIR beam is then linearly polarised and focussed into a vacuum chamber for UV generation, resulting in a spatially approximately Gaussian beam with a beam waist of $65\mu$m at the focus. The chamber contains a glass chip made of fused silica ($SiO_2$), a gas inlet and a pumping system. Its specifications are central to the THG process and are described in more detail in the following.

The fused silica chip is equipped with a laser machined central 3mm-long channel with a 0.5mm diameter. Pressurised gas, normally Argon or Neon, is pumped through the channel, with a two-stage differential pumping system on both sides of the central interaction region ensuring a tight confinement of the gas in this region. As the pump beam passes through the cell and interacts with the pressurised gas THG takes place, which results in UV pulses being generated. The UV components are then separated from the pump beam upon exiting the vacuum chamber using dispersive mirrors, which reflect in the UV but transmit in the NIR. Figure 1a shows a simplified schematic of this set-up, without the pumping system. The fused silica chip, including the two pumping stages is shown in Figure 1b, with the 3mm central interaction region highlighted.

The fused silica chip shown in Figure 1b is an improved design on a simpler fused silica cell which
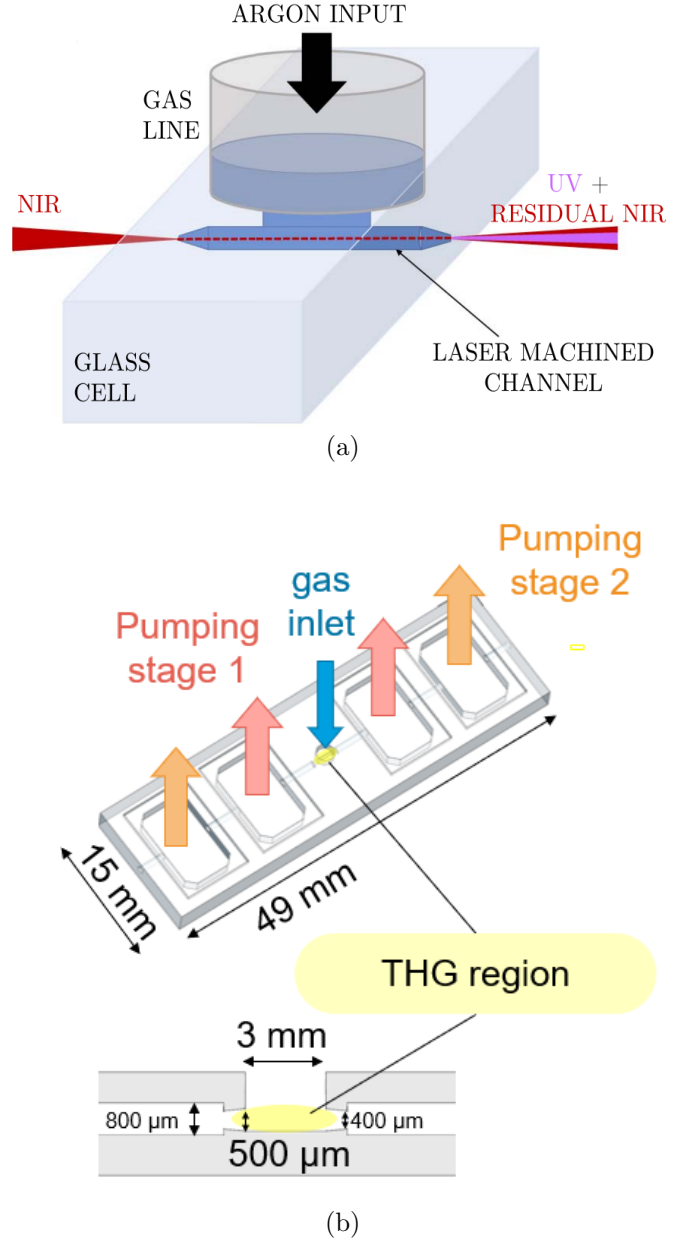


(a)



(b)

Figure 1: The fused silica chip used to confine the gas for THG. Figure 1a shows a simplified schematic of the THG process taking place in the glass cell, without the pumping system, while Figure 1b gives a detailed overview of the chip's design. XXX IMAGE CREDIT

was used previously. The old and new cell have the same 3mm central interaction region but in the old design pumping took place further from the gas inlet, resulting in a less tight confinement of the gas in the THG region. Experimental results demonstrate that the new chip outperforms the old when it comes to UV energies and pulse durations. How this can be related to the difference in gas distribution between the two designs will be explored later. Note that all measurements presented in this report were taken with the new

chip in place.

## 3. Simulation Results

In order to reproduce the experimental conditions described in Section 2.4 as closely as possible in the simulations the simulation input was based on measured data, wherever possible. Thus, the time-frequency information as well as the central wavelength of the NIR input pulse used to model the pump beam in the simulations were read in from experimental data. Spatially, the input beam was assumed to be a Gaussian with a beam waist and focus position corresponding to the values used experimentally.

Apart from the profile of the NIR input beam, the most important THG condition to be modelled was the gas density distribution in the fused silica chip. A fully realistic model of the gas distribution, taking into account the geometry of the chip as well as the effects of the differential pumping system, is challenging to obtain. Some efforts to achieve this have been made using the *COMSOL Multiphysics* software but no sufficiently accurate model of the gas distribution throughout the entire chip could be produced at this point. Therefore, the THG simulations focused exclusively on the 3mm central interaction region of the chip. The density distribution in this region was modelled using a gradient based on the central pressure at the gas inlet and the pressure at the edges of the central interaction region, which has been measured to be around 1mbar. The gradient model is based on an interpolation of pressure values between the central and the edge pressure using the equation

$$P(z)^2 = P(z_0)^2 + (z - z_0)\frac{P(z_1)^2 - P(z_0)^2}{z_1 - z_0}, \quad (10)$$

where $z$ is a point on the between $z_0$ and $z_1$, which are two points at which the pressure is known, such as the centre and edges of the THG region. The density distribution is then inferred from the interpolated pressure distribution.

While discrepancies between this simplified density model and the real distribution are to be expected, especially due the lower-density regions just outside the cell, in which relevant pulse-shaping and absorption processes likely take place, being ignored, the gradient model of the central interaction region can be expected to at least provide qualitatively meaningful results.

In Section XX, the simulations are extended outside the central interaction region in order to compare the performance of the new chip with that of the old cell. The density distributions used in these cases are based on *COMSOL Multiphysics*

simulations of the gas flow. As mentioned above, these simulations are only approximate at the present stage, as they do not sufficiently take into account the interactions between gas molecules in the high pressure regions. Thus, the comparison between the cells is a qualitative one. Note that both the old and the new cell are modelled equally well by the gradient model.

While the simulations can be run for a variety of different gases, central pressures and input beam powers, the results presented in this report will, for simplicity, mostly focus on Argon at 150mW NIR power and Neon at 400mW NIR power, with central gas pressures of 0.4bar and 2.0bar, respectively. These values were chosen due to the availability of high quality experimental data at these parameters.
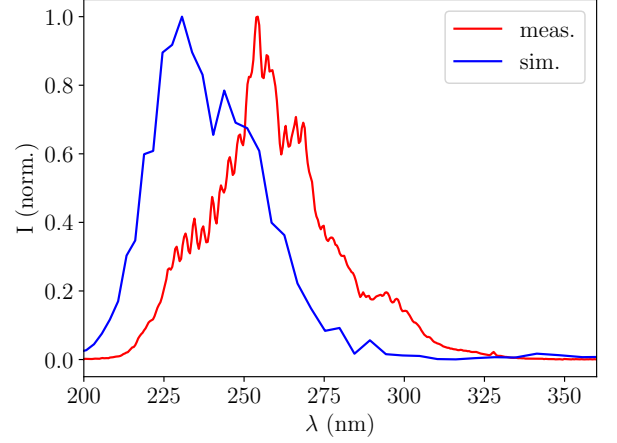
### 3.1. Comparison with Experiment

This section compares some of the simulation output with experimental data.

As can be seen in Figure 2, there is good qualitative agreement between the simulated and measured UV output pulse energies for both Argon and Neon. The energy axes for both plots are normalised to allow for a better qualitative comparison despite a discrepancy between the simulated and measured energies by a factor of roughly ten. This overestimation of the UV energies in the simulation can likely be attributed to the simplistic gas density distribution used, which, for example, does not take into account UV absorption in the low-density regions outside the cell. Similarly, the pressure values for the simulated data had to be rescaled by a factor of 2.5 in both cases to compensate for a mismatch between measured and simulated pressures. The origin of this mismatch, apart from the shortcomings of the gradient model, is the experimental challenge associated with finding an absolute pressure value at the gas inlet, which is why therefore usually approximated with the pressure at the gas pump (???). Taking into account these factors, however, the simulations can clearly reproduce general trends concerning the relationship between UV energies and cell pressure, despite using the simplified gradient model.
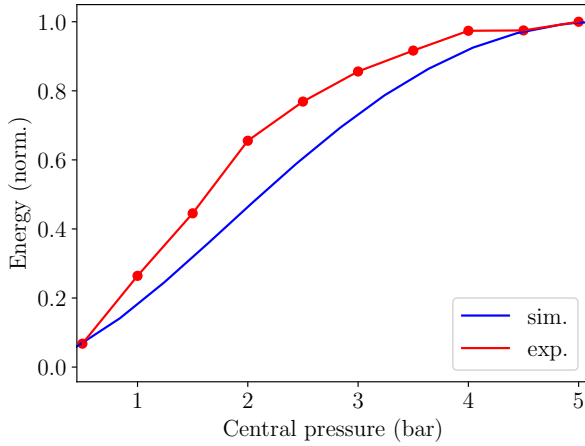
Figure 2 shows that in both simulations and experiment, UV energies rise with increasing central pressure. This is due to higher pressures being associated with higher gas densities in the cell and hence more polarisable gas atoms, increasing the nonlinear polarisation response and hence the effective value of $\chi^{(3)}$. At higher pressures, the trend slows down and eventually reverses because of ionisation effects: the UV beam in the gas
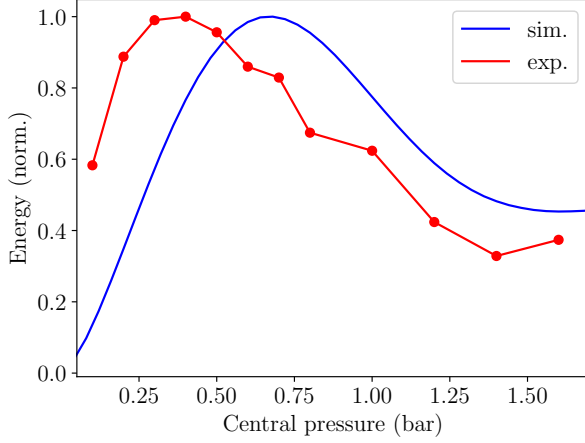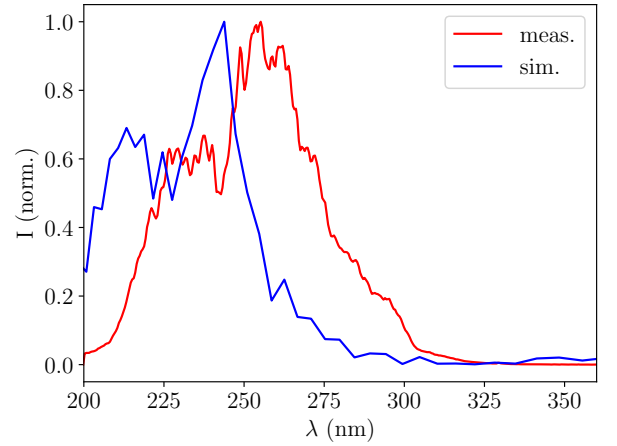
(a) Argon at 150mW NIR beam power



(b) Neon at 400mW NIR beam power

Figure 2: Simulated and experimental values for UV output energies at different central pressures. Note that the pressure axes of the simulated data have been rescaled and the energy axes normalised.



(a) Argon at 150mW and 0.4bar



(b) Neon at 400mW and 2.0bar

Figure 3: Simulated and measured UV output spectra. The power values in the subfigure captions refer to the NIR beam power and the pressure values to the central cell pressures. Note that the pressures of the simulated spectra have been rescaled.

cell becomes sufficiently intense to contribute to ionisation of the gas atoms, resulting in a depleted output beam. Saturation sets in more quickly for Argon than for Neon due to its ionisation potential being lower and its $\chi^{(3)}$ value being higher.

Beyond the UV energies, it is also instructive to consider the simulated UV output spectra. Figure 3 compares the measured and simulated spectra for both Argon and Neon. Despite the shortcomings of the gradient model, the spectra are in remarkable agreement, with most significant features of the experimental spectra reproduced in the simulations. As expected, the spectra are centred on roughly 266nm, corresponding to the third harmonic of the central wavelength (800nm) of the NIR input beam. A comparison of simulated and experimental UV spectra across different central pressures is shown in Figure 4. The simulations clearly

reproduce the general trend of higher pressures resulting in a gradual red-shift. Some discrepancies between simulated and measured data are also apparent, however, like the simulations predicting the splitting of the central peak for Argon and the saturation of UV intensities in Neon not being reproduced.

*3.2. Self-steepening and Ionisation*
*3.3. Effects of Chirp*
*3.4. Comparison of Cells*
section 1: comparison with experiment; section 2: investigate additional parameters; section 3: gas cell
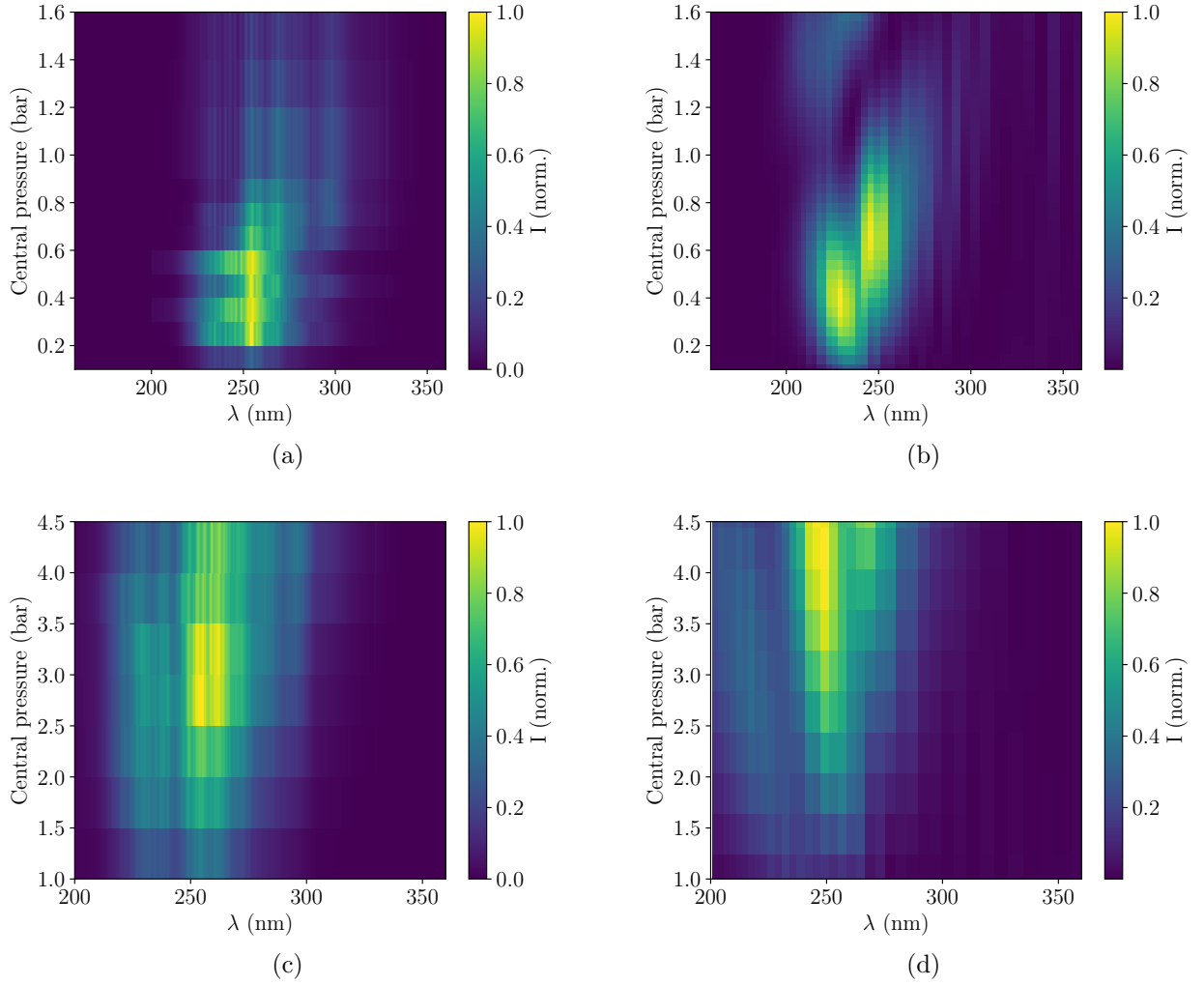
[8]

Figure 4: UV output spectra at different central pressures. Measured data is shown in the left column, simulated data with rescaled pressure axes in the right column. The top row corresponds to Argon at 150mW NIR power while the bottom row correspons to Neon at 400mW NIR power

## 4. Discussion

The THG simulations produced as part of this project yielded some promising results: qualitative agreement with experimental data and the literature could be observed. Indeed, some of the figures presented in this report will be used in a manuscript submitted to the *Journal of Physics: Photonics.*

There is significant room for further improvement of the simulations. For instance, the measured spatial profile of the NIR input pulses could be fed into the simulations, replacing the Gaussian approximation as well as the assumption of radial symmetry. As the input beam shape and its potential defects, like astigmatisms, have been shown experimentally to affect UV generation it is likely that implementing this degree of freedom in the simulations would have a significant effect. Most importantly, the THG simulations should be extended beyond the 3mm central interaction region in

the chip. As the preliminary comparison between the old and new chip in Section 5 showed, the gas density profile outside the central interaction region seems to have a significant effect on UV generation. A better model of the gas distribution, taking into account nonlinear optical effects as well as absorption outside the central chamber might resolve the misalignment of the simulated and measured energy scales: the preliminary *COMSOL Multiphysics* gas distributions show a change in UV energies compared to considering only the central interaction region of an order of magnitude. Whether the simulated and measured pressure scales can be aligned by an improved gas density model remains to be seen, however, as determining the pressure in the cell is an experimental challenge.

With these improvements, or in their present form, the THG simulations can be used to explore a wide range of experimental parameters that

influence UV generation. These include different pressure and beam power regimes, a more thorough investigation of the effects of a chirped input beam, as well as different gases.

Given sufficient future modification and calibration, the THG simulations have the potential to become useful tools in evaluating experimental data as well as theoretically exploring the effects of changing various experimental parameters.

## 5. Conclusion
This report presented
!!!

summarise everything

## Acknowledgments

I want to thank Josina Hahne for supervising the project and all of her support as well as Vincent Wanie for his additional guidance. I also want to thank Chris Brahms for providing help with *Luna.jl* and the entire CFEL-ATTO group for being so welcoming and friendly. Finally, thank you to Olaf Behnke and Andreas Przystawik for organising the DESY Summer Student programme.

## References

[1] M. Galli, V. Wanie, D. P. Lopes, E. P. Månsson, A. Trabattoni, L. Colaizzi, K. Saraswathula, A. Cartella, F. Frassetto, L. Poletto, F. Légaré, S. Stagira, M. Nisoli, R. M. Vázquez, R. Osellame, and F. Calegari, "Generation of deep ultraviolet sub-2-fs pulses," Opt. Lett. **44**, 1308–1311 (2019).
https://opg.optica.org/ol/abstract.cfm?URI=ol-44-6-1308

[2] C. Brahms and J. C. Travers, "Luna.jl," (2023).
https://doi.org/10.5281/zenodo.8242646

[3] U. Keller, *Ultrafast lasers: a comprehensive introduction to fundamental principles with practical applications* (Springer, Cham, Switzerland, 2021).

[4] G. New, *Introduction to Nonlinear Optics* (Cambridge University Press, 2011).

[5] M. Geissler, G. Tempea, A. Scrinzi, M. Schnürer, F. Krausz, and T. Brabec, "Light Propagation in Field-Ionizing Media: Extreme Nonlinear Optics," Phys. Rev. Lett. **83**, 2930–2933 (1999).
https://link.aps.org/doi/10.1103/PhysRevLett.83.2930

[6] M. Kolesik and J. V. Moloney, "Nonlinear optical pulse propagation simulation: From Maxwell's to unidirectional equations," Phys. Rev. E **70**, 036 604 (2004).
https://link.aps.org/doi/10.1103/PhysRevE.70.036604

[7] F. Tani, J. C. Travers, and P. S. Russell, "Multimode ultrafast nonlinear optics in optical waveguides: numerical modeling and experiments in kagome photonic-crystal fiber," J. Opt. Soc. Am. B **31**, 311–320 (2014).
https://opg.optica.org/josab/abstract.cfm?URI=josab-31-2-311

[8] F. Reiter, U. Graf, E. E. Serebryannikov, W. Schweinberger, M. Fiess, M. Schultze, A. M. Azzeer, R. Kienberger, F. Krausz, A. M. Zheltikov, and E. Goulielmakis, "Route to Attosecond Nonlinear Spectroscopy," Phys. Rev. Lett. **105**, 243 902 (2010).
https://link.aps.org/doi/10.1103/PhysRevLett.105.243902